AJNR

CSF Flow Studies of Intracranial Cysts and Cyst-like Lesions Achieved Using Reversed Fast Imaging with Steady-State Precession MR Sequences

Karl T. Hoffmann, Norbert Hosten, Bernd U. Meyer, Simone Röricht, Christian Sprung, Johann Oellinger, Matthius Gutberlet and Roland Felix

AJNR Am J Neuroradiol 2000, 21 (3) 493-502
http://www.ajnr.org/content/21/3/493

AJNR Am J Neuroradiol 21:493–502, March 2000

CSF Flow Studies of Intracranial Cysts and Cyst-like Lesions Achieved Using Reversed Fast Imaging with Steady-State Precession MR Sequences

Karl T. Hoffmann, Norbert Hosten, Bernd U. Meyer, Simone Röricht, Christian Sprung, Johann Oellinger, Matthius Gutberlet, and Roland Felix

BACKGROUND AND PURPOSE: **Differentiating between intracranial cysts or cyst-like structures and communicating or noncommunicating cysts is often not possible with cranial CT or nonfunctional MR imaging. We evaluated a retrospective ECG-gated fast imaging with steady-state precession (PSIF) MR sequence with optional cine mode to differentiate cystic masses from enlarged CSF spaces and to determine the accuracy of detecting communication between cysts and neighboring CSF spaces.**

METHODS: **Fourteen patients with intracranial cystic masses underwent CSF flow studies with an ungated and a retrospective ECG-gated cine-mode PSIF sequence in addition to spin-echo imaging. Findings were evaluated retrospectively by using a five-point rating scale and without knowledge of clinical or other imaging findings. Results were compared with intraoperative findings or with results of intrathecal contrast studies.**

RESULTS: **Eighteen arachnoid cysts and one enlarged cisterna magna were diagnosed. Improved differentiation between cysts and enlarged CSF spaces was obtained with cine-mode PSIF imaging in six lesions (six patients). Increased diagnostic certainty as to communication between cysts and CSF spaces was obtained in 18 cysts (13 patients). Diagnoses were verified by membranectomy in five lesions, by CT cisternography in five lesions, and indirectly by shunting in one cystic lesion. In one case, MR diagnosis was not confirmed by CT cisternography.**

CONCLUSION: **Cine-mode MR imaging with a retrospective ECG-gated flow-sensitive PSIF sequence contributed to the certainty of communication between arachnoid cysts and neighboring CSF spaces with an accuracy of 90%, using surgical findings or intrathecal contrast studies as reference. Differentiation between intracranial cysts and enlargement of CSF spaces and other cystic masses was improved in 25% of cases.**

Classification of circumscribed areas of enlargement of compartments of the CNS that have CSF-like signal intensity or density sometimes presents a differential diagnostic problem, especially when the question of possible communication between arachnoid cysts and neighboring CSF spaces arises. Such enlargements or cysts may be situated extra-axially, as with arachnoid cysts, intraventricularly (eg, colloid cysts), or intraparenchymally (eg, parasitic infections, cystic metastases). Cranial CT and MR imaging studies sometimes do not provide sufficient information about whether circumscribed intracranial or intraspinal enlargements are true cysts or merely enlargements of CSF spaces, although imaging characteristics of arachnoid cysts have been described (1). Diagnostic uncertainty applies in particular to the existence of a membrane between CSF-containing compartments. Such small membranes may be invisible on MR images owing to the transmission of physiologic pulsations between CSF and the brain. It would be useful to resolve this problem, especially in regard to patients with functional impairment of the cranial nerves, symptoms of increased intracranial pressure, or deficits related to spinal cord dysfunction (2).

Ventriculography and CT cisternography (CTC) are invasive functional techniques used for the diagnosis of arachnoid cysts (2). Sensitivity of MR imaging to slow pulsatile CSF flow has been de-

Received April 9, 1999; accepted after revision September 24.

From the Departments of Radiology (K.T.H., N.H., J.O., M.G., R.F.), Neurology (B.U.M., S.R.), and Neurosurgery (C.S.) Charité, Campus Virchow-Klinikum, Humboldt-University, Berlin, Germany.

Address reprint requests to Karl T. Hoffmann, MD, Strahlenklinik und Poliklinik, Charité, Campus Virchow-Klinikum, Augustenburger Platz 1, D-13353 Berlin, Germany.

scribed by a number of authors (3–12). The aim of the present study was to evaluate the usefulness of steady-state free precession (SSFP) MR imaging using a T2-weighted cine-mode reversed fast imaging with steady-state precession (PSIF) sequence as a noninvasive alternative to intrathecal contrast studies for differentiating between arachnoid cysts and enlarged cisterns and for assessing communication between arachnoid cysts and surrounding CSF spaces.

Methods

MR imaging of the brain was performed in 14 patients with a total of 22 intracranial cystic masses. Seven patients were male and seven were female; mean age was 26 years, with a range of 6 to 80 years. One of the patients was examined before and after surgical intervention. Examinations were performed during a period of 4 years on a 1.5-T superconducting system with T1-weighted spin-echo (SE) sequences (500/12/2 [TR/TE/excitations], matrix size = 224 × 256, field of view = 230 mm, slice thickness = 5 mm) and T2-weighted SE sequences (2000/80/1, matrix size = 224 × 256, field of view = 230 mm, slice thickness = 5 mm) in a minimum of two different planes. CSF flow studies were performed with a T2-weighted SSFP sequence (20/25/1, flip angle = 80°, matrix = 256 × 256, field of view = 230 mm, slice thickness = 5 mm, average acquisition time, 11 s) to generate ungated images with static visualization of pulsation-induced flow void. The same sequence parameters were used with an ECG-gated retrospective assignment of data to 15 different periods of a cardiac cycle (average acquisition time, 3.25 min). The reconstructed images (n = 15) showed the real-time dynamic CSF pulsation during a cardiac cycle (cine-mode PSIF) on the screen display.

PSIF is a reversal of the acronym FISP (fast imaging with steady-state precession). These initials are appropriate, because the pulse diagrams of the PSIF sequence (Fig 1A) and the FISP sequence are like mirror images of each other. While the FISP variant is an SSFP sequence with dominating T2* contrast due to gradient echo forming, the PSIF sequence is an SSFP sequence with characteristics of an SE sequence and thus with dominating T2 contrast. This results from the dual function of each RF pulse, which not only excites spins but also owns a refocusing component that acts on the transverse magnetization of the preceding measurement cycle, especially the preceding gradient echo (Fig 1A). In this setting, an SE appears with an effective TE (TE_{eff}) that is longer than the TR (13); this may be called the PSIF echo. In addition to the PSIF echo, a gradient echo (FISP echo) is formed during each cycle; however, only the PSIF echoes are sampled with this sequence (13). A short TR (TR ≪ T2) of RF pulses is a precondition for the maintenance of steady-state transverse magnetization (Fig 1B), whereas retrospective cardiac gating allows a continuous and constant TR during the measurement. The design of the sequence sensitizes it to dephasing effects by moving spins mainly in the readout direction, resulting in an enhanced flow-void phenomenon in the imaging plane (6). The sensitivity of SSFP imaging sequences to slow CSF flow has been described as sufficient for visualizing flow velocity as low as 1 mm/s (3, 10, 11).

Two ungated images with a 90° difference in the direction of flow sensitivity were acquired from every chosen slice position to optimize visualization of in-plane flow. This was achieved by rotating the phase-encoding and readout gradient directions 90° between the measurements (6). Through-plane flow was not specifically sensitized with this technique. The slice orientation of the PSIF sequence was planned with the use of the previously acquired SE images to 1) include the suspected or possible site of a cyst membrane or communication, 2) avoid through-plane orientation of directed flow, and 3) ascertain the most adequate coverage of small cysts in the basal cisterns with respect to the bones of the skull base. During the period in which the cases were collected, no system upgrades were performed that would affect the standard SE sequences, the application, or visualization of the PSIF sequence.

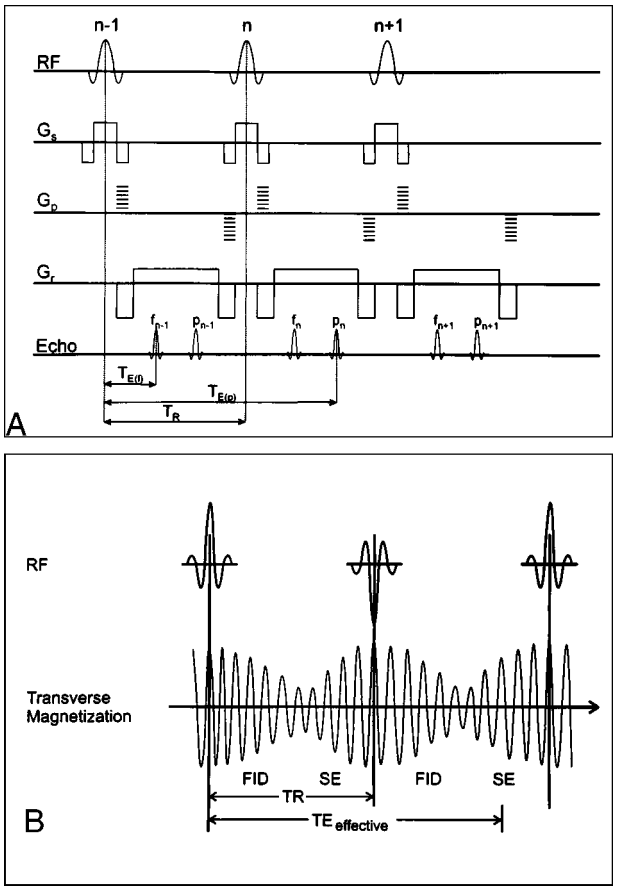

FIG 1. *A,* Diagram of the PSIF pulse sequence. p_n (the PSIF echo) is a spin echo that results from refocusing the echo f_{n-1} by the RF pulse, *n.* f_{n-1} (the FISP echo) is a gradient echo of the RF pulse, *n−1,* refocused by the readout gradient, G_r. Only the PSIF echoes are sampled with this sequence. This results in TE_{eff} > TR, with $T_{E(p)} = 2T_R - T_{E(f)}$ in the symmetric arrangement of RF pulses and gradients shown. The phase-encoding gradients are applied before and after the echo (including a compensating pulse) for a zero net phase-encoding gradient between RF pulses to avoid affecting the established steady state. Data are sampled during the interpulse interval to avoid interference with RF transmission (6).

B, Alternating RF pulses and oscillating transverse magnetization in relation to the free induction decay (*FID*) and spin echo (*SE*) in SSFP imaging with the PSIF sequence.

Preparation of ungated PSIF images for evaluation included adjusting the window and center at the monitor and filming the thus-optimized images. Thereafter, images were evaluated visually from the film. The cine-mode studies, with a frequency of five to six images per second, were read directly from the monitor.

The differential diagnoses of the cases were assessed retrospectively by two interpreters using a rating scale to differentiate cysts from enlarged cisterns: 0, no cyst; 1, probably no cyst; 2, uncertain; 3, probably a cyst; 4, cyst. Another rating scale was used to judge communication between arachnoid cysts and neighboring CSF spaces: 0, no communication; 1, probably no communication; 2, uncertain; 3, probably com-

munication; 4, communication. By means of this rating scale, and using only conventional MR images, the interpreters first differentiated between an intracranial cystic mass and an enlarged CSF space, and between communicating and noncommunicating cysts. Afterward, we investigated whether the diagnosis changed and whether diagnostic certainty was raised when CSF flow studies were taken into account. Therefore, the ungated PSIF images and, in a third step, the cine-mode PSIF studies, were analyzed. A diagnostic improvement of one point on the rating scale, for example, may reflect the change from uncertain (2 points) to probably no cyst (1 point), or from probably communication (3 points) to communication (4 points), and would be marked by a positive sign (+1). A numerical change with a negative sign would indicate a change from a more certain to a less certain diagnosis.

The results were compared with clinical symptoms, operative findings (six cysts), and CTC findings (six cysts). In one patient with two cysts, both CTC and membranectomy were performed. Criteria for communication on CT cisternograms included visualization of intracystic contrast enhancement or an unequivocal increase in Hounsfield units (HU) within the cyst (by at least 300% relative to plain films) at 20 to 30 minutes or up to 3 hours after intrathecal contrast application on delayed scans.

Results

T1- and T2-weighted SE images showed 19 intracranial cysts or cystic lesions in the 14 patients (Table 1). When CSF flow studies were taken into account to establish a definitive diagnosis, 18 intracranial arachnoid cysts and one enlarged cisterna magna were diagnosed.

The intracranial locations of the arachnoid cysts were frontal (n = 1), frontotemporal (n = 1), temporal (n = 5), suprasellar (n = 2), prepontine (n = 1), pontocerebellar (n = 5), paramedullar (n = 1), and paracerebellar (n = 2). In seven cases (four pontocerebellar and two temporal arachnoid cysts and one excessively enlarged cisterna magna), the findings were incidental, without definite correspondence to clinical symptoms (Fig 2).

Six of the cystic lesions in three patients were associated with developmental malformations (Chiari II malformations, congenital aqueductal stenosis combined with hypothalamic hamartoma, and aqueductal stenosis with dysplasia of the corpus callosum).

Differentiation between Cysts and Enlarged CSF Spaces

The differential diagnosis between intracranial cyst and enlarged CSF space improved with the use of ungated PSIF images in five cysts in five patients (+5 points on the rating scale relative to SE images). Use of cine-mode PSIF imaging produced no further increase in certainty in these five patients. Ungated and cine-mode PSIF imaging allowed a definite MR classification of lesions in five cysts in five patients, which had not been possible with SE imaging.

Communication between CSF Compartments

The diagnostic certainty in identifying communication between neighboring CSF compartments was raised for 17 cystic lesions in 12 patients using the ungated PSIF imaging technique (+24 points on the rating scale relative to SE imaging). Using the cine-mode PSIF technique, the certainty increased further (+31 points over SE imaging on the rating scale, or +33 points including the postoperative findings in case 3) for 18 cystic lesions in 13 patients (Fig 2). Compared with ungated PSIF imaging, the cine-mode PSIF technique resulted in a higher diagnostic certainty for seven cystic lesions in six patients, for a total improvement of +7 points on the rating scale (+9 points including the postoperative findings in case 3, see Tables 1 and 2).

Using PSIF and cine-mode PSIF imaging, a predominantly uncertain diagnosis was changed to a definite diagnosis of communication in 16 cysts. The diagnosis was confirmed in nine of the cystic lesions: by membranectomy in five cases (Fig 3), indirectly by shunting in one case, and by CTC in five cases. In one temporal and one frontotemporal cyst (patient 6), the MR diagnosis was confirmed by both CTC (Fig 4) and operative findings. Consistent with MR findings, CT cisternograms showed enhancement and an intracystic increase in HU after intrathecal contrast administration in one temporal cyst (case 14, Fig 5) and a system of one suprasellar and one paracerebellar cyst (case 1, Fig 6) in two other patients. Distinct paths of contrast material within cysts were not identified on CT cisternograms. In another temporal arachnoid cyst (patient 1), results of MR imaging and CTC were judged inconsistent, as the former suggested communication to be unlikely whereas the latter was inconclusive owing to artifacts, with some slight evidence of communication. The diagnoses verified operatively corresponded well with the results of PSIF imaging. Surgically confirmed lesions included one suprasellar, one paramedullar (Fig 3), one paracerebellar, one large frontotemporal, and one temporal arachnoid cyst (Fig 4). External shunting was successfully performed in one frontal arachnoid cyst without evidence of communication on PSIF images and with clinical signs of expansion. An example of a suprasellar cyst is shown in Figure 7.

Discussion

Characterization of CSF-like compartments in the CNS may represent a diagnostic challenge, especially when there is a question of possible communication between arachnoid cysts and neighboring CSF spaces (8, 11). The potential importance of the present study is that SSFP MR imaging with a cine-mode PSIF sequence could be an alternative method by which to clarify differential diagnostic problems in a number of cases, thereby avoiding more invasive and cumbersome procedures, such as CTC.

TABLE 1: Summary of cases

Case No.	Age (yr)/ Sex	MR Findings	Cyst Score*			Communication Score†			Clinical Findings	Confirmation Method
			SE	PSIF	Cine	SE	PSIF	Cine		
1	6/F	Suprasellar cyst	3	4	4	2	3	4	Pubertas precox	Confirmed by CTC
		Temporal cyst	4	4	4	2	1	1	Headache	CTC inconclusive because of artifacts
		Cerebellar arachnoid cyst	4	4	4	2	3	4	. . .	Confirmed by CTC
2	68/F	Pontocerebellar arachnoid cyst	3	4	4	2	1	0	CNV_2 signs, spontaneous remission	. . .
3	44/M	Paramedullar arachnoid cyst	3	4	4	2	1	0	Premembranectomy MR; C.N. VIII signs, paraesthesia of hands/feet, respiratory distress	Confirmed by surgery
				. . .		2	2	4	Postmembranectomy MR	
4	8/F	Megacisterna magna	1	0	0	3	4	4	Incidental finding in epilepsy	. . .
5	7/M	Frontal arachnoid cyst	4	4	4	1	1	0	Headache	Confirmed indirectly by shunting
6	31/F	Frontotemporal cyst	4	4	4	2	4	4	Headache	Confirmed by surgery and CTC
		Temporal arachnoid cyst	4	4	4	2	4	4	. . .	
7	19/F	Pontocerebellar arachnoid cysts	4	4	4	2	0	0	Myoclonus, dysarthric speech, no causal relationship to cysts	. . .
			4	4	4	2	0	0		
8	10/M	Paracerebellar arachnoid cyst	3	4	4	2	4	4	Incidental finding	. . .
9	12/M	Suprasellar arachnoid cyst	4	4	4	2	1	0	Headache, retardation	Confirmed by surgery
10	80/F	Pontocerebellar arachnoid cysts	4	4	4	2	0	0	Myasthenia gravis, no causal relationships to cysts	. . .
			4	4	4	2	0	0		
11	28/M	Prepontine arachnoid cyst	4	4	4	2	1	0	Shunted internal hydrocephalus, occasional headache	. . .
12	18/F	Temporal arachnoid cyst	4	4	4	1	1	1	Suspected psychogenic seizures	. . .
13	7/M	Temporal arachnoid cyst	4	4	4	1	0	0	Incidental finding, besides ipsilateral subdural hematoma after trauma	. . .
14	23/M	Temporal arachnoid cyst	4	4	4	2	3	3	Occasional headaches	Confirmed by CTC

Note.—SE indicates spin-echo sequence; PSIF, ungated fast imaging with steady-state precession sequence; Cine, cardiac-gated cine-mode PSIF seq uence; CTC, CT cisternography; CN, cranial nerve.

* Cyst score: 0, no cyst; 1, probably no cyst; 2, uncertain; 3, probably a cyst; 4, cyst.

† Communication score (of cysts): 0, no communication; 1, probably no communication; 2, uncertain; 3, probably a communication; 4, communication.

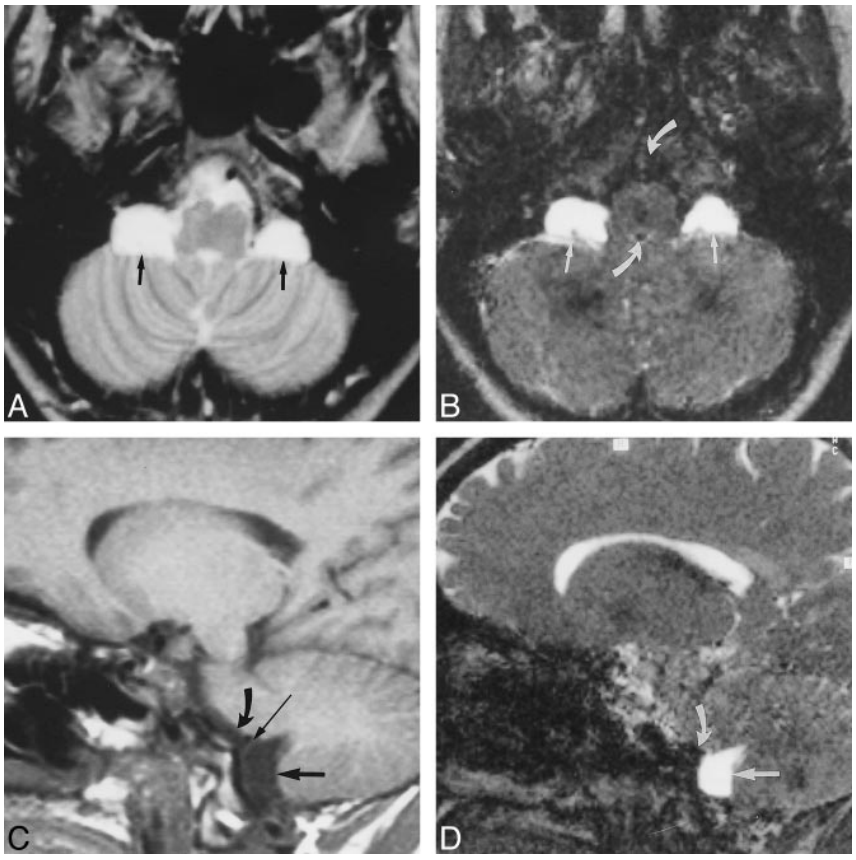

FIG 2. 19-year-old woman with incidentally found arachnoid cysts in the cerebellopontine angle.

A, Transverse T2-weighted SE image (2000/80/1) shows high signal intensity within the enlarged cerebellopontine angles (*arrows*) and in the prepontine cistern. The shape of the enlarged CSF space suggests arachnoid cysts.

B, On the corresponding SSFP image (20/25/1), signal attenuation due to CSF flow is found in the prepontine cistern and fourth ventricle (*curved arrows*). Persistently high signal intensity is found in the cerebellopontine cysts (*straight arrows*) due to stationary CSF, confirming the diagnosis of arachnoid cysts.

C, Sagittal T1-weighted SE image (500/12/2) with suspected thin membrane (*long arrow*) between the isointense subpeduncular space (*curved arrow*) and the left cerebellopontine mass (*short straight arrow*).

D, Corresponding sagittal SSFP image (500/12/2) shows functional separation of the hypointense pulsating CSF between the temporal bone and the cerebellar peduncles (*curved arrow*) and the hyperintense stationary CSF within the cyst (*straight arrow*).

TABLE 2: Summary of lesions in which additional information was obtained from reversed fast imaging with steady-state precession (PSIF) images as compared with spin-echo images

	Ungated PSIF			Cine-Mode PSIF		
	No. of Patients	No. of Lesions	Score*	No. of Patients	No. of Lesions	Score*
General lesion classification (cyst versus non-cyst)	5	5	+5	5	5	+5
Communication	12	17	+24	13	18	+33

Note.—In all, there were 14 patients with a total of 19 lesions.

* Summary of numerical changes in diagnoses after considering ungated and cardiac-gated cine-mode PSIF images. The numerical change in each case results from the difference in points on the rating scale (see Table 1) as determined by findings on SE and PSIF images, with a positive sign for a more certain diagnosis and a negative sign for a less certain diagnosis resulting from the additional use of one of the PSIF techniques.

SSFP imaging techniques are based on a repetitive RF pulse application in the presence of a gradient, which results in periodically alternating magnetization along the gradient. This technique involves flow sensitivity, as the contribution of moving spins to the intensity of an echo depends on their ability to re-establish a new steady state in a finite amount of time. Patz and coworkers (3, 4) earlier introduced an SSFP imaging technique that is sensitive to flow velocities on the order of 1 mm/s and defined a dephasing parameter that could be adjusted to the flow sensitivity depending on the RF interpulse interval, the wavelength of periodic magnetization, and the distance the spin moves during the interpulse interval.

SSFP imaging with the PSIF sequence generates heavily T2-weighted images with reduced T2* effects as compared with other spoiled or refocused gradient-echo techniques, such as fast low-angle shot (FLASH), fast field echo, gradient-recalled acquisition in the steady state (GRASS), or FISP, because the echo of the PSIF sequence is formed by an RF excitation, a process that is unusual for gradient-echo sequences but reduces the influence of local magnetic field inhomogeneities on the spin relaxation. Therefore, the decay of transverse magnetization is dominated by T2. The obtained signal is an SE of the penultimate RF excitation, resulting in the apparent paradox of $TE_{eff} > TR$.

Increased contrast between CSF and brain parenchyma was provided by a relatively large flip angle (80°) and a moderate TE (25 milliseconds). The former increases the contribution of CSF to the transverse magnetization, whereas the latter reduc-

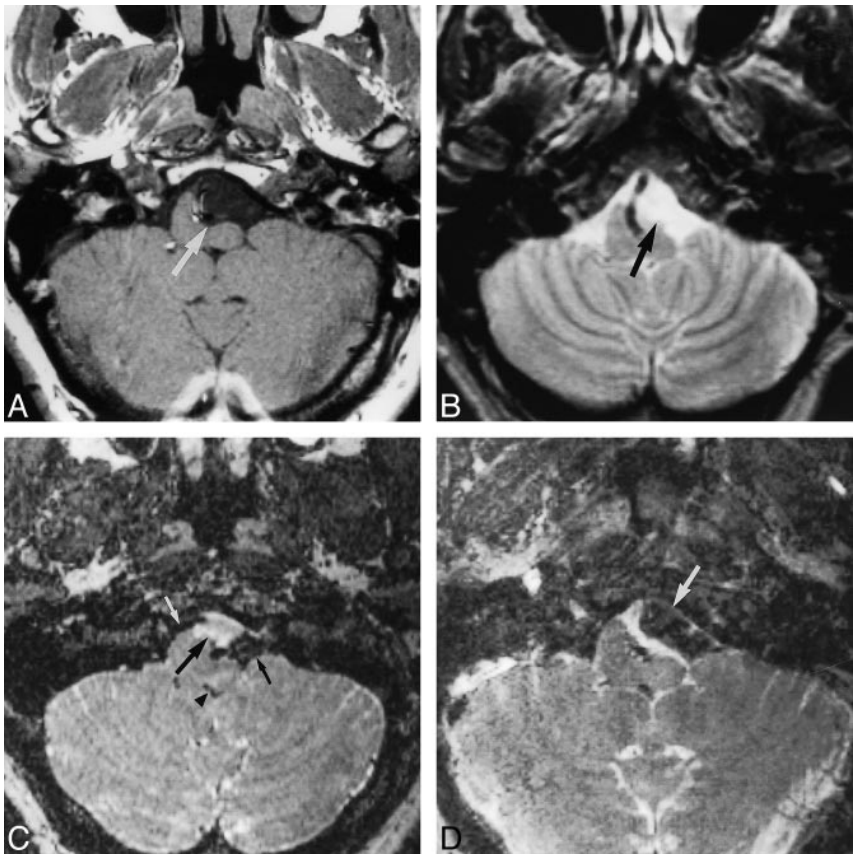

FIG 3. 44-year-old man with left-sided tinnitus and hearing loss, paraesthesia, and respiratory distress.

A, T1-weighted transverse image (500/12/2) of the posterior fossa shows a paramedullary, space-occupying lesion with signal intensity similar to CSF, compressing the left ventrolateral portion of the medulla oblongata (*arrow*).

B, T2-weighted SE image (2000/80/1) of the same section as in *A.* Different compartments are not visible; the lesion has the same signal intensity as the surrounding CSF spaces, and margins of the cyst are not reliably detectable, making the diagnosis of an arachnoidal cyst highly probable.

C, Corresponding preoperative SSFP image (20/25/1) shows a circumscribed, hyperintense, premedullary lesion (*large arrow*), indicating stationary CSF of a noncommunicating arachnoid cyst in contrast to the significantly reduced signal of moving CSF in neighboring compartments (*small arrows*) and in the fourth ventricle (*arrowhead*). This finding strongly supports the decision for neurosurgical intervention.

D, SSFP image (20/25/1) after membranectomy shows signal attenuation in most parts of the formerly hyperintense cyst (*arrow*), indicating communication with neighboring CSF spaces. The patient experienced relief of his symptoms.

es the signal intensity from tissue with moderate T2 relaxation time (<80 milliseconds) (14). The signal intensity of stationary CSF is very high in contrast to the low signal from brain parenchyma. Spin flow due to physiologic CSF pulsation decreases the steady state of transverse magnetization and leads to a marked signal void located adjacent to sites of flow acceleration, such as the foramina of Monro, Luschka, and Magendie, as well as the mesencephalic aqueduct, which is essentially more pronounced than in SE sequences (15).

Retrospective gating allows assignment of continuously obtained imaging data (ie, Fourier lines) to an arbitrarily chosen number of positions within the RR interval of the cardiac cycle and thereafter enables visualization of CSF motion in a cine mode. This technique also facilitates dynamic imaging of slow CSF motion in larger, preformed CSF spaces, such as ventricles or arachnoid cysts. Another possible advantage of cine mode in addition to the ungated PSIF images is that it allows one to visualize intermittent or one-way communication. The ungated sequence may show only the presence or absence of flow, without depicting any abnormal flow dynamics. Making TR independent of cardiac frequency by retrospectively re-sorting Fourier lines guarantees a continuous steady state of the transverse magnetization due to a constant RF pulse rate that would not be possible with prospective triggering without additional sequence preparation (6). Moreover, prospective cardiac gating may require a short interruption of acquisition during each RR interval to detect the next trigger point, which may cause loss of data in the diastolic phase (16).

Other techniques for visualization and assessment of slow CSF flow are diffusion-weighted imaging and phase imaging (9, 10, 17). In a study comparing SSFP and diffusion-weighted imaging in the detection of CSF leaks, Levy et al (9) found diffusion-weighted imaging to be highly sensitive in detecting slow flow, with similar minimally detectable flow rates between the two techniques. Phase imaging can be used to map and quantitate pulsatile flow by allowing measurements of CSF flow direction and velocity, with sensitivity to velocity as slow as 5 mm/s; however, it requires cardiac gating (10, 17). An advantage of SSFP imaging is that it may detect dephasing due to complex flow, whereas phase imaging is intended for laminar flow.

The evaluation of CSF flow with cardiac-gated gradient-echo cine imaging and its ability to discriminate physiologic from abnormal flow patterns, especially in narrow or obstructed CSF pathways (5, 14, 16), and to depict flow communication in cysts (12, 18, 19) has been reported previously. The principles of assessment of CSF flow dynamics with a retrospectively gated, two-dimensional FISP sequence have been described by Nitz et al (16). Kadowaki et al (20) pointed out the meaning of additional functional information on cine MR im-

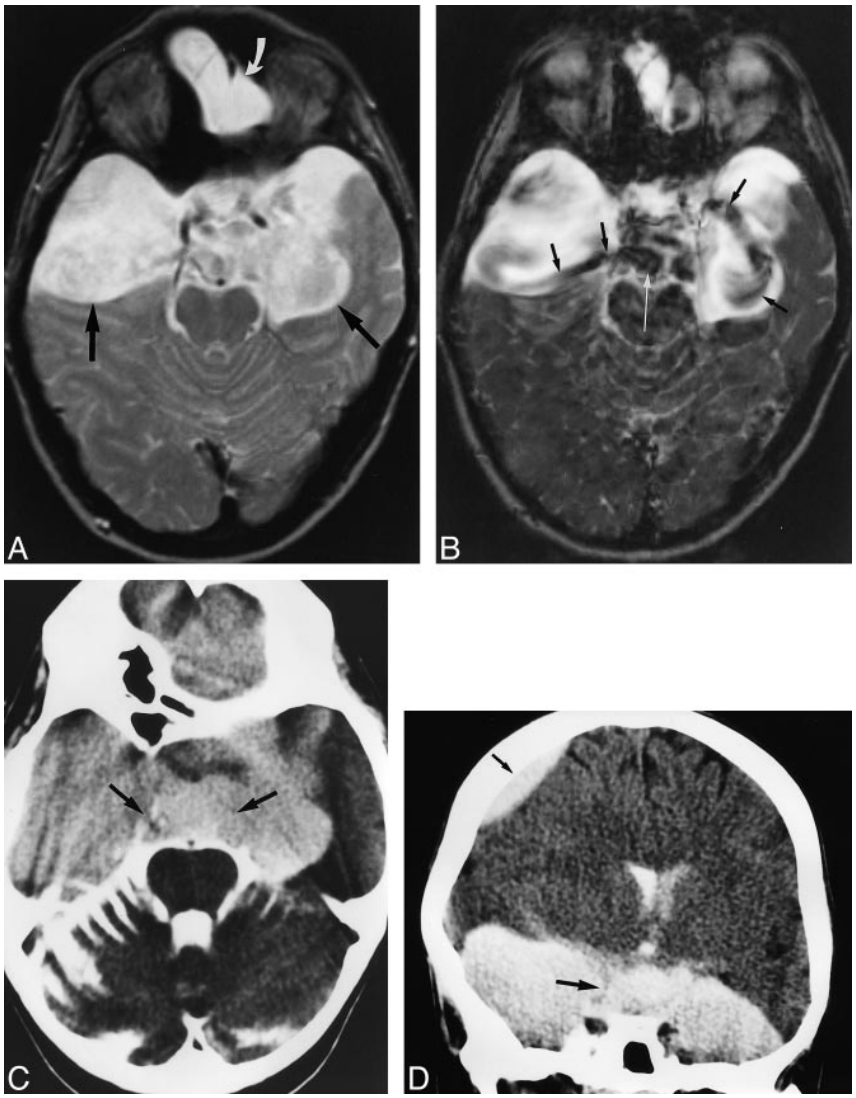

FIG 4. 31-year-old woman after membranectomy of left temporal and right temporofrontal arachnoid cysts.

A, Transverse T2-weighted SE image (2000/80/1) shows slightly inhomogeneous, hyperintense temporal cysts (*straight arrows*). The frontal part of the large right-sided cyst is depicted (*curved arrow*).

B, Corresponding SSFP image (20/25/1) of the same section clearly shows a jet phenomenon with distinct signal reduction arising from the right prepontine and left chiasmatic cisterns, indicating communication between the cysts and cisterns (*black arrows*). Marked signal reduction results from moving CSF in the prepontine cistern (*white arrow*). The contents of the arachnoid cysts appear, with local flow attenuation, more inhomogeneous in the SSFP image (20/25/1) owing to higher sensitivity to turbulent flow.

C and *D,* Transverse (*C*) and coronal (*D*) CT cisternograms show homogeneous contrast enhancement within the basal cisterns and both the left temporal and right temporofrontal cysts. The regions of bilateral membranectomy are indicated by *arrows.* The coronal image also shows a frontal part of the right cyst (*small arrow*).

aging beyond the ungated, static depiction in the assessment of aqueductal stenosis and occlusion. Schellinger et al (10) described different flow velocity patterns in various degrees of spinal canal compromise.

To confirm communication between CSF-containing compartments, the depiction of a jet-like flow void at the assumed communication site proved to be the most convincing criterion (Fig 4). This kind of locally restricted flow acceleration was visible on the ungated PSIF images, but the cine-mode PSIF technique improved the ability to distinguish it from pulsatile movements, which were transmitted throughout a thin but continuous layer separating adjoining cavities. The occurrence of a marked and clearly defined signal difference between a homogeneous hyperintense cyst and a dark neighboring CSF space proved to be the most important argument against communication. This difference was found mainly with relatively small cysts near the brain stem, cerebellum, and skull base (Fig 2), where surrounding CSF pulsation seemed naturally more pronounced than in the supratentorial compartments, because of the increased compression of the more caudal brain structures with systole (21). The flow void on PSIF images exceeded in every case the corresponding signal loss on T2-weighted SE images. Eguchi et al (12) reported time-of-flight and phase-contrast cine MR imaging with a two-dimensional FLASH sequence in 10 patients with arachnoid cysts of the middle fossa. They also found jet flow and marked pulsatile signal alteration within the cyst to be decisive criteria for communication of arachnoid cysts. Santamarta et al (22) reported a single case with endoscopically confirmed valve-like communication of a suprasellar arachnoid cyst. Enzmann et al (19), in an analysis of fluid pulsations in spinal cord cavities of patients with syringomyelia, found different flow patterns, indicating pulsatile and nonpulsatile cysts. These authors described a reduction of pulsatile flow in shunted cavities on postoperative imaging studies. A possible explanation for this observation may lie in the differences in CSF flow dynamics between spinal cavities in syringomyelia (also described with a water-hammer model) and

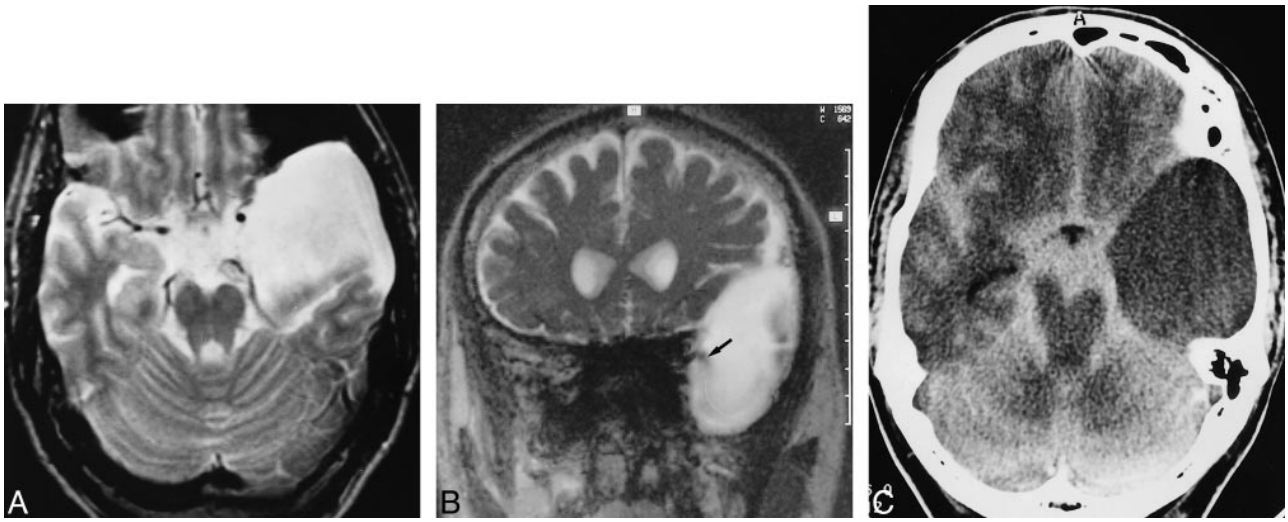

FIG 5. 23-year-old man with a left-sided temporal arachnoid cyst, suffering from occasional headaches.

A, Transverse T2-weighted SE image (2000/80/1) shows a hyperintense left temporal arachnoid cyst.

B, Coronal PSIF image (20/25/1) depicts distinct signal reduction (*arrow*) arising from the basal cisterns, indicating probable communication.

C, CT cisternogram (3-hour delay) shows slight contrast enhancement within the cyst, confirming slow communication. The contrast enhancement was confirmed by measuring a clear increase of intracystic HU. The site of communication was not detectable on the CT cisternogram owing to proposed valve mechanism with slow communication.

arachnoid cysts, with reduction of intracavity turbulent flow after shunting in syringomyelia. Pulsatile flow void was evaluated on long-TR, long-TE, selective-saturation-recovery gradient-refocusing, and GRASS images, reflecting methodologic approaches without implications for cine MR imaging. Fujimura et al (23) reported superior sensitivity of cine MR imaging as compared with conventional MR imaging in the evaluation of an intradural arachnoid cyst.

Investigating the differentiation between simple cysts, cyst-like tumors, and hemorrhagic cysts, Tien et al (14) found SSFP images to provide additional information. These authors described increased contrast of non-CSF-like contents relative to stationary CSF in cysts, and improved differentiation between solid and hemorrhagic tumor components and perifocal edema relative to that seen on SE images. Owing to the relatively homogeneous appearance of arachnoid cysts with CSF-like contents

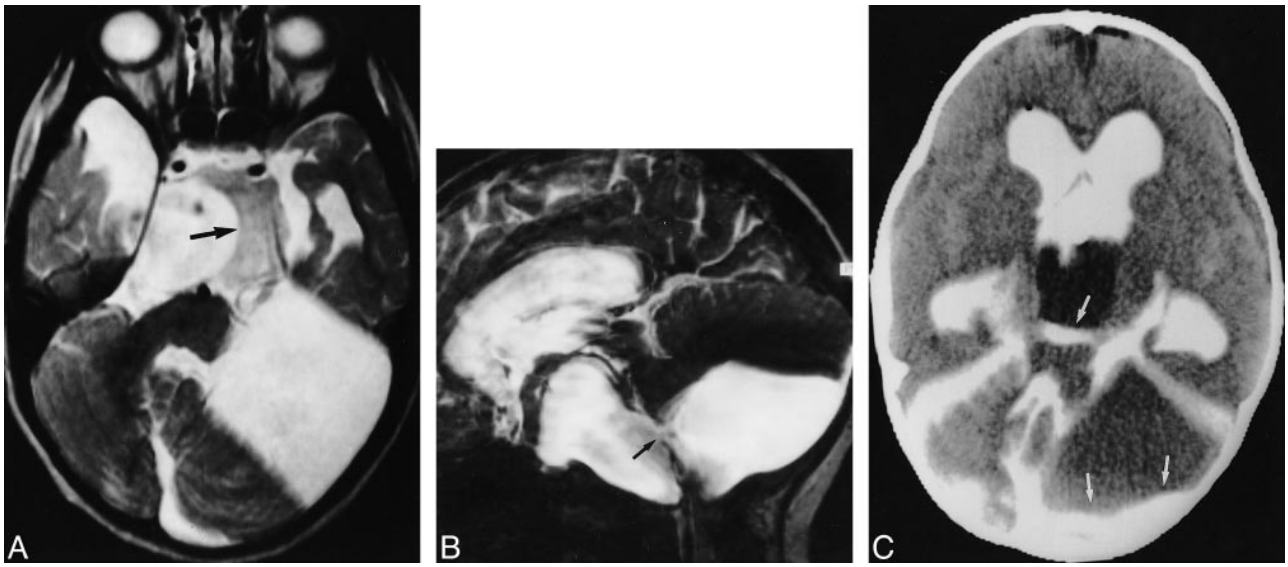

FIG 6. 6-year-old girl with a system of temporal, supra- and parasellar, and paracerebellar arachnoid cysts.

A, Transverse T2-weighted SE image (2000/80/1) shows a right and small left temporal, suprasellar, and paracerebellar cysts. Note hamartoma of the tuber cinereum (*arrow*) anterior to the rotated brain stem.

B, Parasagittal PSIF image (20/25/1) shows some evidence of communication between the parasellar and paracerebellar cysts in the form of a continuous flow void (*arrow*).

C, CT cisternogram shows contrast enhancement with layering in the parasellar and paracerebellar cysts (*arrows*), providing further evidence of communication. Layering was caused by the patient's prolonged supine position.

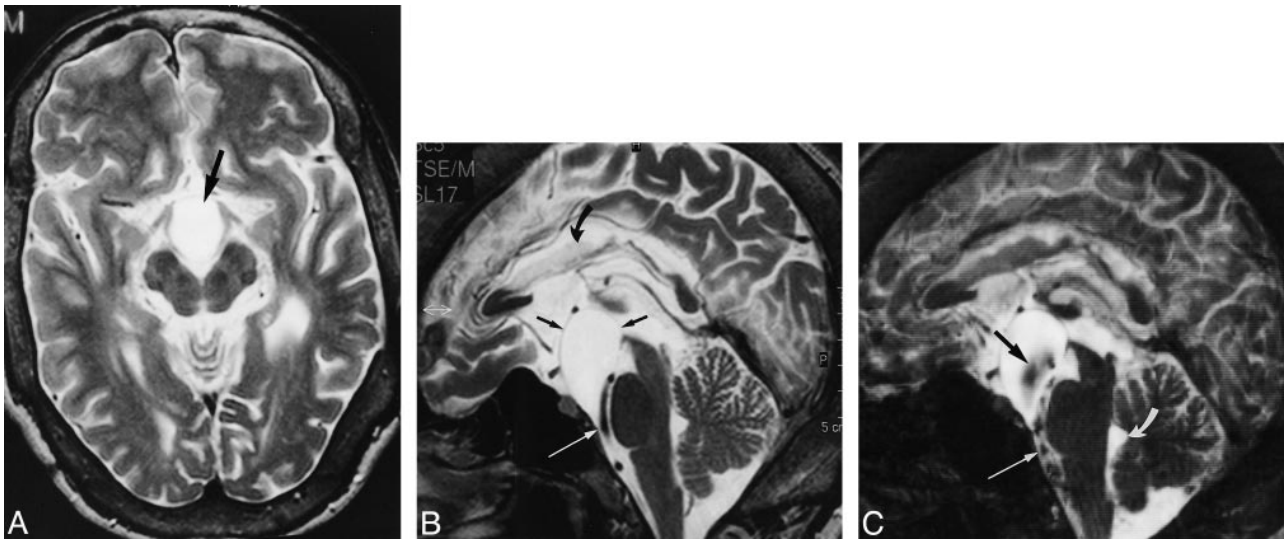

FIG 7. 28-year-old man with a prepontine arachnoid cyst, corpus callosum anomaly, hydrocephalus, ventriculoperitoneal shunt, and headaches.

A, T2-weighted axial image (2000/80/1) shows a hyperintense cyst (*arrow*) within the prepontine cistern, pushing the crura cerebri and the optic chiasm apart.

B, Midsagittal T2-weighted section (2000/80/1) shows defined margins of the cyst (*straight black arrows*), except for the narrowing between the basilar artery and skull base (*white arrow*). Note callosal dysplasia (*curved arrow*). The bottom of the third ventricle is elevated.

C, Midsagittal SSFP image (20/25/1) reveals broad-based signal void within the cyst (*black arrow*) probably due to transmission of pulsations from the basilar artery. A continuous jet phenomenon between the prepontine cistern with pronounced signal void (*straight white arrow*) on the one hand and the cyst on the other hand is not demonstrable, making communication unlikely. Flow void within the fourth ventricle was absent (*curved arrow*) owing to occlusion of the aqueduct. Membranectomy was not performed, because the patient had no evidence of visual impairment.

and otherwise enlarged CSF spaces, which were the focus of our study, additional imaging with the PSIF sequence proved most effective in determining whether there was communication with arachnoid cysts. The occurrence of flow voids in cysts also depends on the pliability of the cyst walls and the effectiveness with which transmitted CSF pulsations cause geometric deformation of the cyst. False-positive PSIF findings may be attributable to transmission of CSF pulsation throughout the intact cyst wall with flow void outside and inside the cyst, mimicking communication. Failure to recognize true communication between a cyst and neighboring compartments may result from incomplete coverage of the cyst by the scan volume or unsuitable slice orientation, with a possible jet flow perpendicular to the plane of single slices. In case of restricted communication with CSF pathways, diffusion may lead to considerably delayed enhancement of the cyst contents on CT cisternograms (24). This would probably be interpreted as a noncommunicating cyst on an MR flow study. Shunting of an expanding cyst, however, would be an appropriate treatment both in restricted and absent communication (24). On the basis of their results with CTC, Crisi et al (2) suggested the following classification scheme: rapidly communicating or false cysts (with communication between cyst and subarachnoid space) or slowly communicating or true cysts (with no communication), because only slow or noncommunicating cysts tend to expand and cause serious neurologic disorders.

Although, in a number of cases, our results did not correspond to operative findings or to findings on other imaging studies, we think they indicate that ungated and cine-mode SSFP imaging with the retrospective ECG-gated PSIF sequence offers a clear tendency toward increased diagnostic accuracy in the evaluation of intracranial and spinal cysts; in particular, arachnoid cysts and cyst-like lesions.

Conclusion

For some cases, we regard a CSF flow study with a cine-mode PSIF technique as a noninvasive alternative to CTC for functional evaluation of arachnoid cysts, because it enables visualization of flow communication between cysts and neighboring CSF compartments. This technique can be useful in preoperative evaluation of questionable expanding cysts, in follow-up after membranectomy, and in differentiating merely enlarged physiologic CSF spaces from cysts. Cine-mode CSF flow studies may also contribute to a better clinical understanding of regional abnormalities in individual patients.

Acknowledgment

We wish to thank Bernard C. Sander, M.D., from the Department of Radiology at Charité, Berlin, for his contribution to sequence implementation.

References

1. Wiener SN, Pearlstein AE, Eiber A. **MR imaging of intracranial arachnoid cysts.** *J Comput Assist Tomogr* 1987;11:236–241
2. Crisi G, Calo M, De Santis M, Angiari P, Merli GA. **Metrizamide-enhanced computed tomography of intracranial arachnoid cysts.** *J Comput Assist Tomogr* 1984;8:928–935
3. Patz S, Hawkes RC. **The application of steady-state free precession to the study of very slow fluid flow.** *Magn Reson Med* 1986;3:140–145
4. Patz S. **Some factors that influence the steady state in steady-state free precession.** *Magn Reson Imaging* 1988;6:405–413
5. Jolesz FA, Patz S, Hawkes RC, Wallman JK. **Mapping of normal and abnormal cerebrospinal fluid flow/motion patterns using steady state free precession imaging.** *Acta Radiol Suppl (Stockh)* 1986;369:302–304
6. Jolesz FA, Patz S, Hawkes RC, Lopez I. **Fast imaging of CSF flow/motion patterns using steady-state free precession (SSFP).** *Invest Radiol* 1987;22:761–771
7. Jolesz FA, Patz S. **Clinical experience with rapid 2DFT SSFP imaging at low field strength.** *Magn Reson Imaging* 1988;6: 397–403
8. Davis SW, Levy LM, Le Bihan DJ, Rajan S, Schellinger D. **Sacral meningeal cysts: evaluation with MR imaging.** *Radiology* 1993; 187:445–448
9. Levy LM, Gulya AJ, Davis SW, Le Bihan DJ, Rajan SS, Schellinger D. **Flow-sensitive magnetic resonance imaging in the evaluation of cerebrospinal fluid leaks.** *Am J Otol* 1995;16:591–596
10. Schellinger D, Le Bihan D, Rajan SS, et al. **MR of slow CSF flow in the spine.** *AJNR Am J Neuroradiol* 1992;13:1393–1403
11. Brooks ML Jolesz FA, Patz S. **MRI of pulsatile CSF motion within arachnoid cysts.** *Magn Reson Imaging* 1988;6:575–584
12. Eguchi T, Taoka T, Nikaido Y, et al. **Cine-magnetic resonance imaging evaluation of communication between middle cranial fossa arachnoid cysts and cisterns.** *Neurol Med Chir* 1996;36: 353–357
13. Bruder H, Fischer H, Graumann R, Deimling M. **A new steady-state imaging sequence for simultaneous acquisition of two MR images with clearly different contrasts.** *Magn Reson Med* 1988;7:35–42
14. Tien RD, McFall J, Heinz R. **Evaluation of complex cystic masses of the brain: value of steady state free-precession MR imaging.** *AJR Am J Roentgenol* 1992;159:1049–1055
15. Quencer RM, Post MJ, Hinks RS. **Cine MR in the evaluation of normal and abnormal CSF flow: intracranial and intraspinal studies.** *Neuroradiology* 1990;32:371–391
16. Nitz WR, Bradley WG, Watanabe AS, et al. **Flow dynamics of cerebrospinal fluid: assessment with phase-contrast velocity MR imaging performed with retrospective cardiac gating.** *Radiology* 1992;183:395–405
17. Enzmann DR, Pelc NJ. **Cerebrospinal fluid flow measured by phase-contrast cine MR.** *AJNR Am J Neuroradiol* 1993;14:1301–1307
18. Levy LM, Di Chiro G. **MR phase imaging and cerebrospinal fluid flow in the head and spine.** *Neuroradiology* 1990;32:399–406
19. Enzmann DR, O'Donohue J, Rubin JB, Shuer L, Cogen P, Silverberg G. **CSF pulsations within nonneoplastic spinal cord cysts.** *AJR Am J Roentgenol* 1987;149:149–157
20. Kadowaki C, Hara M, Numoto M, Takeuchi K, Saito I. **Cine magnetic resonance imaging of aqueductal stenosis.** *Childs Nerv Syst* 1995;11:107–111
21. Enzmann DR, Pelc NJ. **Brain motion: measurement with phase-contrast MR imaging.** *Radiology* 1992;185:653–660
22. Santamarta D, Aguas J, Ferrer E. **The natural history of arachnoid cysts: endoscopic and cine-mode MR evidence of a slit-valve mechanism.** *Minim Invasive Neurosurg* 1995;38:133–137
23. Fujimura M, Tominaga T, Koshu K, Shimizu H, Yoshimoto T. **Cine-mode magnetic resonance imaging of a thoracic intradural arachnoid cyst: case report.** *Surg Neurol* 1996;45:533–536
24. Wolpert SM, Scott MR. **The value of metrizamide CT cisternography in the management of cerebral arachnoid cysts.** *AJNR Am J Neuroradiol* 1981;2:29–35